River Flow 2010 - Dittrich, Koll, Aberle & Geisenhainer (eds) - © 2010 Bundesanstalt für Wasserbau ISBN 978-3-939230-00-7

Coherent turbulence structure generated by wind-induced water waves

M. Sanjou, I. Nezu & A. Toda
Department of Civil Engineering, Kyoto University, Katsura Campus, 615-8540, Kyoto, Japan

ABSTRACT: It is very important for global environment problems to reveal turbulence characteristics and coherent structure generated by wind-induced water waves. Some previous studies pointed out that the turbulence generation depended on phases of water waves, in which single-point measurements of a laser Doppler anemometer (LDA) were conducted intensively. However, there remain uncertainties about the effects of wave phases on coherent turbulence motion, e.g., ejections & sweeps, and streaky structure. Simultaneous measurements of velocities and free-surface elevation allow us to conduct reasonably the phase analysis of the coherent structure in interfacial shear layer. Particularly, multi-point measurements such as PIV are very powerful to detect the space-time structure of coherent motions. Therefore, in the present study, we developed a specially designed PIV system which can measure the velocity components and surface-elevation fluctuations simultaneously by using two sets of high-speed cameras to reveal the coherent structure in the interfacial shear layer between water and wind.

Keywords: Wind-induced water waves, Coherent structure, Air/water interface, PIV measurements

1 INTRODUCTION

In ocean and natural lakes, water waves and turbulence are generated by wind. Particularly, mass / momentum transport and gas exchanges are promoted significantly beneath the interface between the air and water. It is, therefore, very important for many environment problems to investigate turbulence structure and coherent eddies related to such mass and momentum transport.

It is well known that a large-scale low-pressure system overlying an ocean causes significant water waves. Toba et al. (1996) revealed that wind-induced water waves generate "down-bursting", which is accompanied by strong downflows in the subsurface. The down-bursting has a lower frequency than the wave period and has significant effects on the air/water interface, e.g., flow resistance, turbulence generation, and mass and momentum exchanges. These wind-induced waves often appear in both natural rivers and artificial open channels. Early, Rashidi & Banerjee (1990) focused on turbulence structure in open-channel flow, where the velocity shear was imposed on the free-surface by wind. They revealed that main characteristics of the low-speed streaky structure are similar to those near the wall, even though the boundary conditions at the wall and at the air/water interface are quite different from each other. Komori et al. (1993) indicated that a surface renewal eddy and down-bursting are associated with the production of the velocity shear, water waves and separation / reattachment of the wind over the free surface.

Many previous studies conducted single-point measurements of a laser Doppler anemometer (LDA) and acoustic Doppler velocimetry (ADV), and pointed out that the turbulence generation has a significant relationship with water waves. For example, Cheung & Street (1988) used a linear filtering technique (LFT), in which the wave motion is evaluated by cross spectra of velocity and free surface fluctuations, and they suggested that there exists a significant energy transfer from the wave to the mean flow. They have also shown that the turbulence structures at the presence of wind-waves have similar characteristics to those observed in turbulent boundary layers. In contrast, Jiang et al. (1990) proposed a stream function method (SFM), in which the wave motion is assumed to be a potential flow. They have revealed that the interaction between wave and turbulence plays a vital role on energy transfer mechanism between them. These previous studies offered many valuable knowledges and database to consider statistical properties of turbulence related to the wind-induced waves. However, there

Table 1. Hydraulic condition

H (cm)	H_s (cm)	$U_{a,\max}$ (m/s)	U_s (cm/s)	U_* (m/s)
4	0.4	6.8	28.1	0.0169

remain uncertainties concerning the effects of wave phases on coherent turbulence motion. Recently, Oh et al.(2008) analyzed the time-series of vorticity distributions by using PIV measurements, and found that coherent structure is transported associated with wave motions. Sanjou et al. (2009) have conducted phase analysis on the basis of PIV data to reveal turbulence generation mechanism under water waves. To investigate coherent turbulence structure in more detail, we need simultaneous measurements of velocities and free-surface elevation to conduct reasonably the phase analysis of the coherent structure in interfacial shear layer. Therefore, in the present study, we developed a specially designed PIV system which can measure the velocity components and surface fluctuation simultaneously by using two sets of high-speed cameras.

2 EXPERIMENTAL METHOD

2.1 *Simultaneous measurement setup of velocity components and free-surface profile*

The experimental setup is indicated in Fig.1. The experiments were conducted in a 16m long and 40cm width × 50cm height glass-made wind-tunnel flume. In this flume, air-flow is generated over the free-surface flow by a speed-controlled fun. x and y are the streamwise and vertical coordinates, respectively. The vertical origin, $y = 0$, was chosen as the channel bed. The time-averaged velocity components in each direction are defined as U and V, the corresponding turbulent fluctuations are u and v, respectively. 2W laser light sheet (LLS) was projected from the flume bottom. The $x-y$ plane was illuminated with tracer particles and it was taken by a pair of high-speed CMOS cameras(1000 × 1000 pixels, 500frame/s). To measure the velocity components and surface elevation simultaneously, two high-speed cameras are used for the PIV measurements and free-surface capture, respectively.

The hydraulic conditions are shown in Table 1. The measurement area is 7m downstream of the upstream entrance. In this study, the water depth was 4cm and the maximum wind speed $U_{a,\max}$ was 6.8m/s in order to generate gravity waves. H_s is the significant wave height. U_s is the velocity at the air-water surface evaluated from the ensemble averages of 30 samples with 3mm float. U_* is the friction velocity of water side evaluated from the logarithmic-law.

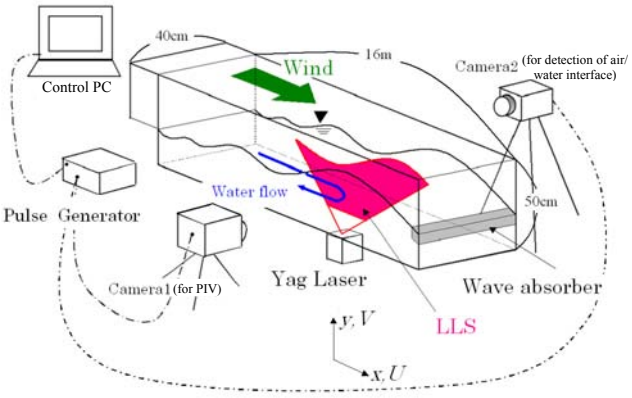

Figure 1. Experimental setup

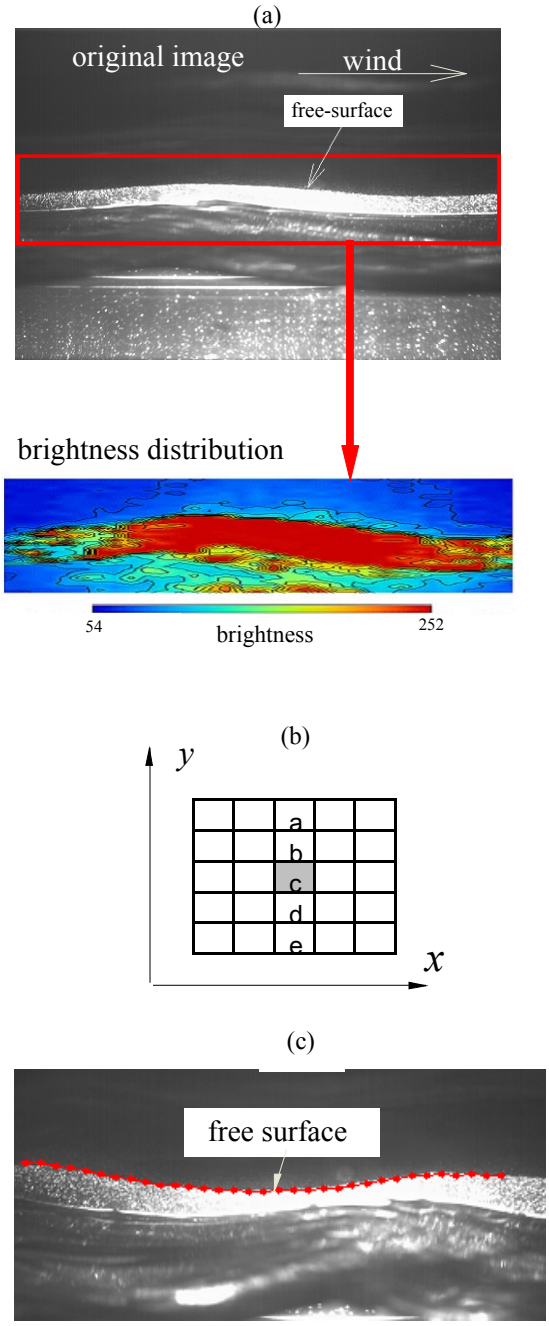

Figure 2. Detection process of air/water interface.
(a) original image and the corresponding brightness distribution, (b) definition of pixel locations and (c) evaluated distribution of air/water interface

2.2 *Detection process of air/water interface*

We applied a method proposed by Miyamoto et al.(2002) to detect the air/water interface. To extract the air/water interface exactly, the picture images taken by the present CMOS camera should be in good condition of focus and clearness. We dissolved Rhodamine-B in the present flume water to rise up clearness near the boundary between air-water interfaces. Fig.2(a) shows the original image and brightness distribution, in which we can see discern the water and air layers by eyes. Using the brightness data at each analyzing mesh point, we obtain the brightness gradient in the vertical direction which is defined as follows;

$$G_c = a + 2b - 2d - e \qquad (1)$$

in which, the points "a" to "e" are the local brightness data as shown in Fig.2(b).

After calculation of G_c, considering five points in the y-direction, the center point P_c is chosen as the 1st-candidate point(1st-C point) of borderline, if P_c is the largest among them. This process is conducted at each streamwise location. Then, we sort out the 2nd-candidate points from the 1st-C points using two thresholds (H_{TV}, L_{TV}) in the following way. First,1st-C point which is larger than H_{TV} is detected. The modified images composed of such 1st-C points is called as "Seedmap". Secondly, we search the 2nd-C points that meet the following conditions.

(1)They are one of the1st-C points.
(2)They are located next to already detected 2nd-C points on the Seedmap.
(3)The brightness gradient is larger than L_{TV}.

The above mentioned calculation was continued, and finally, all points on the Seedmap could be considered as air/water interface. Fig.2(c) shows an example of the free-surface curve plotted in the original image picture. It was found that the calculated interface curve agreed well with that observed in the original image.

3 RESULTS AND DISCUSSIONS

3.1 *Spectrum of free-surface fluctuations*

Fig.3 shows the spectra of free-surface fluctuations obtained by the above-mentioned method, in which the result of capacitance-type wave-gauge was also shown for comparison. In the present method, the spectra were calculated at two different points, i.e., the center of image $(x/L_x = 0)$ and the right-hand-side edge of image $(x/L_x = 1)$. L_x is the half length of image in the streamwise direction. It is found that the spectral peak obtained by the present method agreed with that obtained by the wave gauge. A lot of noises appear in the case of edge position $(x/L_x = 1.0)$ of the image compared to the center position $(x/L_x = 0)$, and this is because the light power of LLS not strong enough to obtain good results near the edge of images.

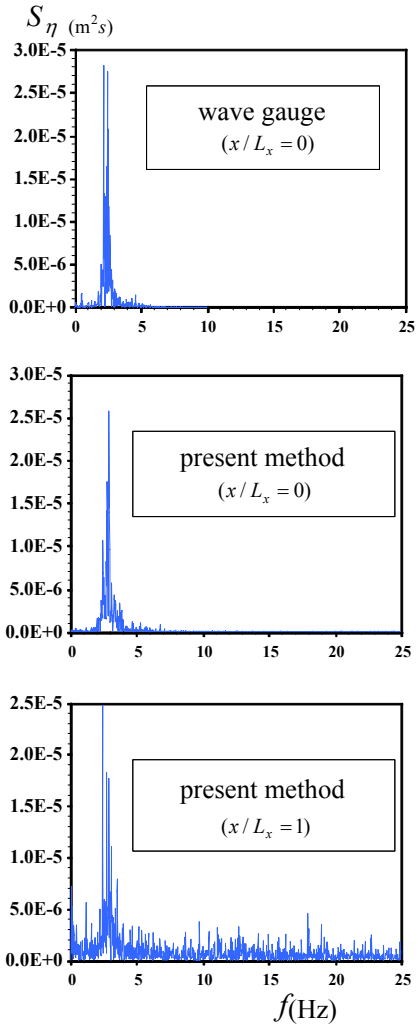

Figure 3. Spectrum of free-surface fluctuations. Comparison between the present method and wave-gauge result

3.2 *Streamwise velocity and turbulence profiles*

Figs.4(a), (b) and (c) show the vertical profiles of time-averaged streamwise velocity, turbulence intensities and Reynolds stress, respectively. A large velocity gradient $\partial U/\partial y$ is observed near the free surface $(y/H > 0.8)$, and in contrast, a return flow $(U < 0)$ is formed significantly between $y/H = 0.6$ and 0.85.

This large velocity shear influences turbulence intensities, i.e., $u' \equiv \sqrt{\overline{u}^2}$ and $v' \equiv \sqrt{\overline{v}^2}$. It was found in all cases that the larger turbulence is generated more significantly closer to the water surface. Furthermore, u' and v' became larger with an increase of wave height. In 2-D gravity wave conditions, the vertical component was larger than the streamwise component near the free surface, i.e. $v' > u'$. This property is quite different from that observed in wall boundary layers, and thus it is peculiar to turbulent flow under the wind-induced water waves. Any influence of water waves

appears significantly even in the Reynolds stress. That is to say, there exist negative values of $-\overline{uv}$ near the free-surface associated with phase lag of streamwise and vertical components of velocity. This property has

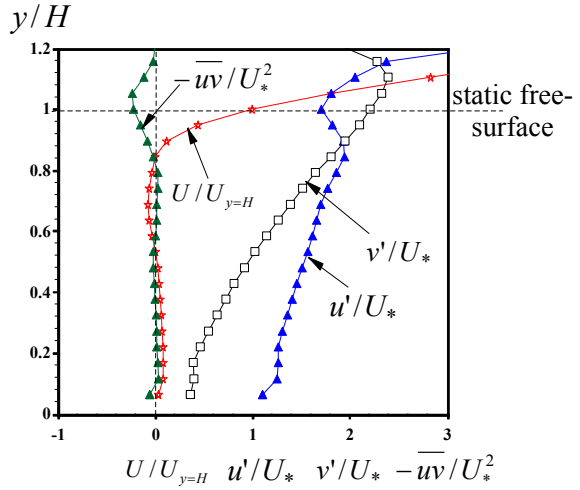

Figure 4. Profiles of time-averaged streamwise velocity, turbulence intensities and Reynolds stress

been reported by previous studies, e.g., Cheung & Street (1988).

3.3 *Instantaneous properties of velocity components*

Fig.5 shows the time-variations of instantaneous velocity vectors and free-surface boundary at every 0.04 seconds, in which the color contour means the streamwise $\tilde{u}$ and vertical $\tilde{v}$ components for (a) and (b), respectively. It should be noticed that the crest and trough of waves are transported downstream with time. One can see downflows $(V<0)$ in the backward side of crest and upflows $(V>0)$ in the forward one. In contrast, the downflow and upflow are observed in the forward and backward sides of trough, respectively. Furthermore, these fluid parcels of upflows and downflows are convected downstream together with wave propagation. It is found from the contours of streamwise velocity that the large velocity zones are located near the crest, and in contrast, return flow zones are formed in the trough. These fluid parcels are also transported downstream. The vertical velocity component becomes almost zero at the crest and trough, and positive and negative values appear alternatively in the transition stages between the crest and trough.

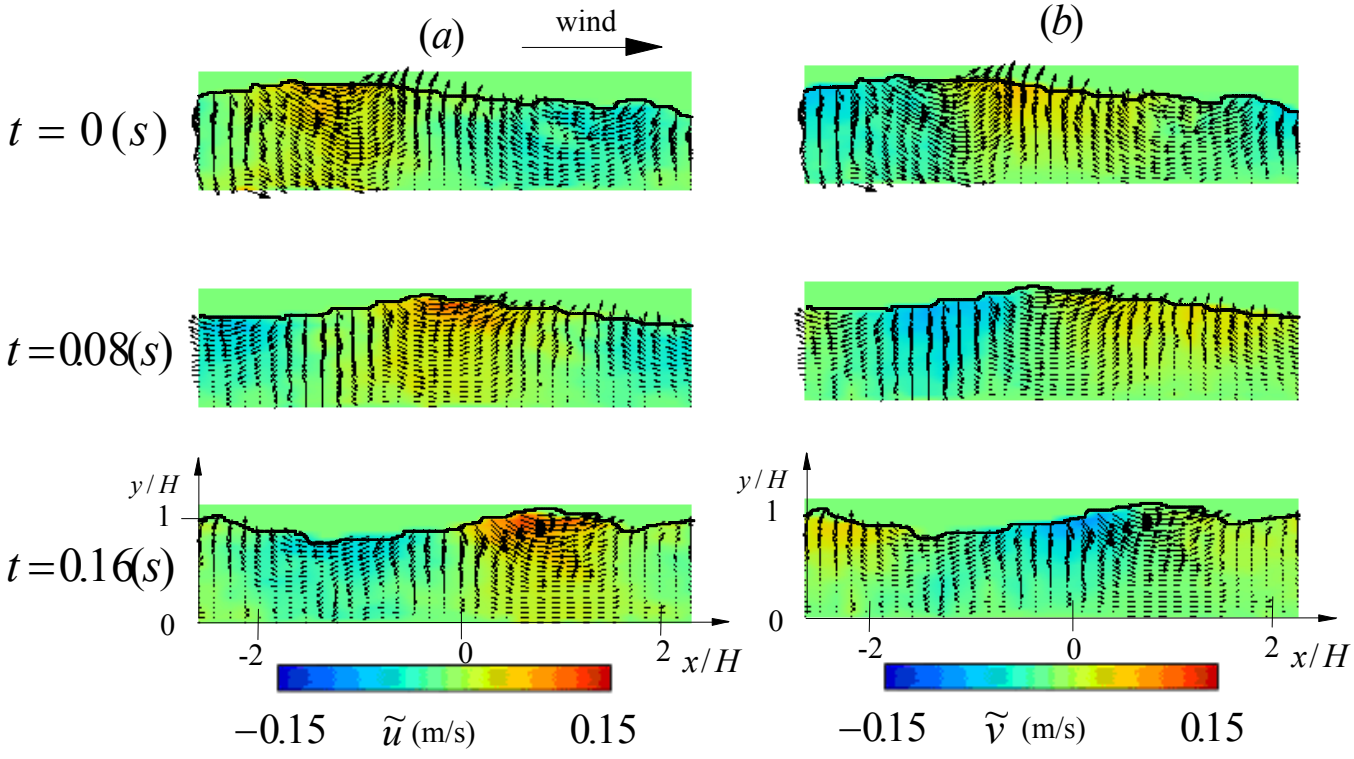

Figure 5. Instantaneous velocity vectors and free-surface distributions, (a) streamwise velocity and (b) vertical velocity

Fig.6 shows the time-series of velocity components and free-surface fluctuation $\tilde{\eta}(t)$ at one point of x=0 and y/H=0.5. As mentioned above, there exists a strong correlation between the velocity components and free-surface fluctuation, that is to say, $\tilde{u}$ becomes maximum at the crest, and $\tilde{v}$ becomes minimum at the trough stage. Although, the periodicities of streamwise and vertical velocity components are almost same, there exists phase-lag that is about a quarter of wavelength.

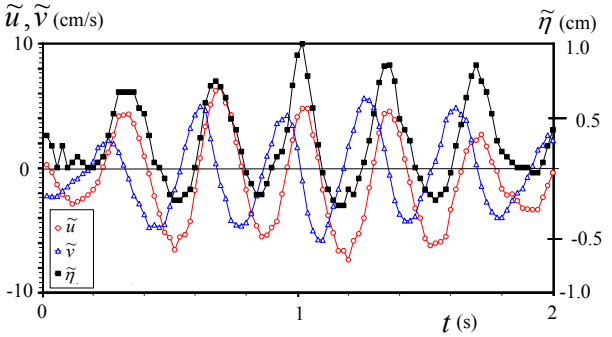

Figure 6. Time-variations of velocity components $(\tilde{u}, \tilde{v})$ and free-surface elevation $\tilde{\eta}$, (x=0, y/H=0.5)

3.4 *Correlation between velocity components and free-surface fluctuations*

Fig.7 shows the correlation between the velocity component and free-surface fluctuation, in which the reference position was chosen by the center of image, i.e. $x_0 = 0$. The correlations between free-surface fluctuations $\tilde{\eta}$ at $x_0 = 0$ and velocity components at movable positions, $C_{\eta u}(x, y)$ and $C_{\eta u}(x, y)$, are defined as follows:

$$C_{\eta u}(x,y) = \frac{\overline{(\tilde{\eta}(x_0,t) - \overline{\eta}(x_0)) \times (\tilde{u}(x,y,t) - \overline{u}(x,y))}}{\eta'(x_0) \times u'(x,y)} \tag{2}$$

$$C_{\eta v}(x,y) = \frac{\overline{(\tilde{\eta}(x_0,t) - \overline{\eta}(x_0)) \times (\tilde{v}(x,y,t) - \overline{v}(x,y))}}{\eta'(x_0) \times v'(x,y)} \tag{3}$$

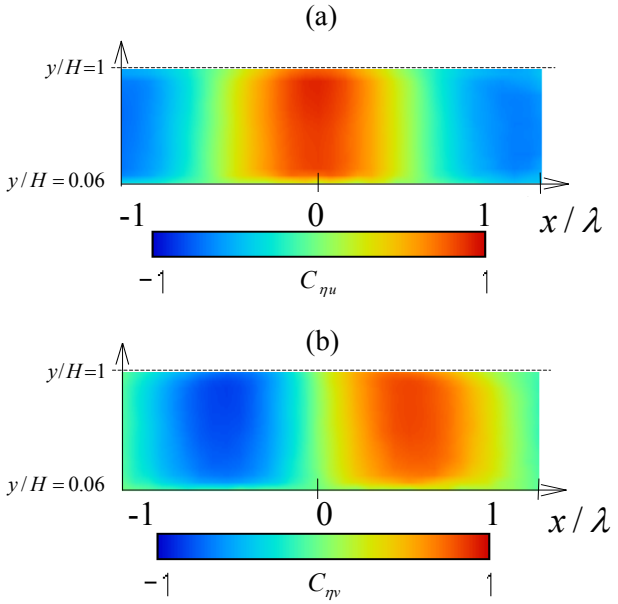

Figure 7. Distribution of correlation function, (a) correlation between streamwise velocity and free-surface fluctuation and (b) vertical component and free-surface fluctuation

in which, the over bar means time-average operation. It is found that $C_{\eta u}$ has maximum value at the reference position, $x/\lambda = 0$ and minimum value at $x/\lambda = \pm 1$, in which λ is the wave lenght. This implies that the streamwise velocity varies with same phase with waves. Whereas, $C_{\eta v}$ becomes maximum at $x/\lambda = 0.5$ and minimum at $x/\lambda = -0.5$. This property is almost same in the whole depth region. These results suggest that there is a phase lag between the vertical velocity and waves.

3.5 *Coherent turbulent vortex*

Oh et al.(2008) pointed out an existence of coherent vortex structure by using the following instantaneous vorticity. Fig.8 shows the time-variations of the instantaneous vorticity, $\tilde{\omega}(t) \equiv \partial\tilde{u}/\partial y - \partial\tilde{v}/\partial x$. At t=0(s), a strong positive parcel exists in the crest zone, and the vorticity is larger in the forward side of the crest than in the backward one. This property agrees well with the results proposed by Okuda (1982). The crest region is convected downstream accompanied with the strong vorticity parcel as time passes. In contrast, at t=0.16(s), the vorticity is smaller in the forward side than the backward one. This may be because convection velocity of coherent vortex differs from the Stokes drift velocity.

Some researchers have proposed several mathematical methods to detect the vortex core of coherent structure in shear layers and mixing layers. One of them is the delta method proposed by Chong & Perry (1990). They considered the eigenvalues σ of the velocity shear tensor $(\partial\tilde{u}_i/\partial x_j)$ in shear layers. The eigenvalue equation in 2-D shear flow is given by

$$\sigma^2 - P\sigma + Q = 0 \tag{4}$$

in which,

$$P \equiv \frac{\partial\tilde{u}_i}{\partial x_i} = 0 \tag{5}$$

$$Q \equiv \frac{1}{2}\left(\left(\frac{\partial\tilde{u}_i}{\partial x_i}\right)^2 - \frac{\partial\tilde{u}_i}{\partial x_i}\frac{\partial\tilde{u}_j}{\partial x_j}\right) \tag{6}$$

and

$$\Delta \equiv P^2 - 4Q \tag{7}.$$

$\tilde{u}_i$ is the instantaneous velocity component. Complex eigenvalues occur when the discriminant Δ is negative. It is assumed that $\Delta < 0$ corresponds to an existence of vortex core. Fig.9 shows the distribution of Δ which corresponds to Fig.8. At t=0(s), a large-scale vortex zone is observed between the crest and trough. At t=0.04 to 0.08 (s), a vortex is generated in the downstream side of the crest. Furthermore, at t=0.08 to 0.16 (s), another vortex is observed at the left-hand-side of Fig.9, and this location corresponds to the transition zone from the trough to the crest. Of particular significance is that the coherent vortex is generated

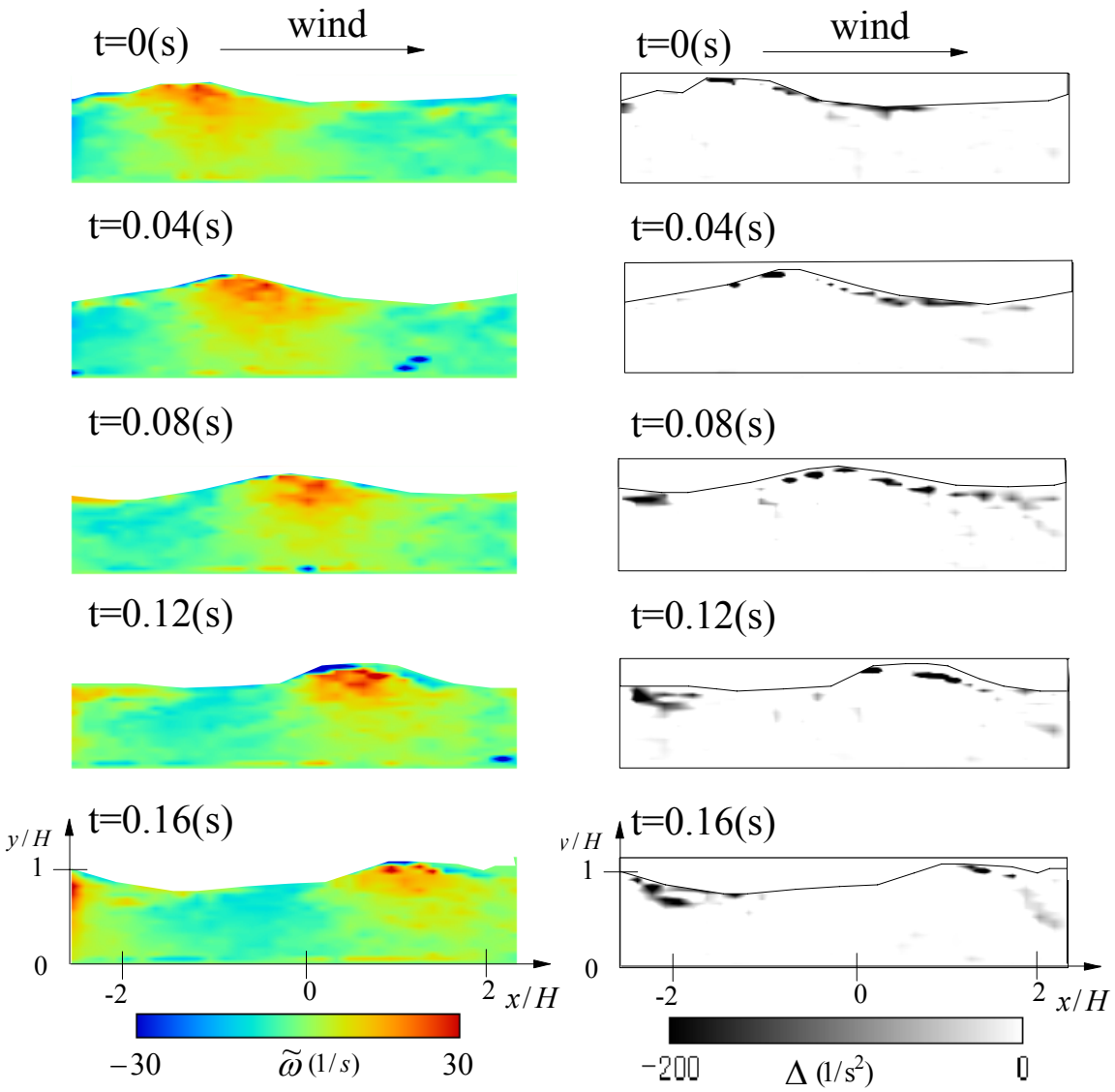

Figure 8. Time-variation of vorticity distribution

Figure 9. Time-variation of delta distribution

significantly in the transition stage between the crest and the trough.

3.6 *Phase analysis of turbulence generation*

Phase analysis is very useful to reveal the effects of free-surface fluctuations on turbulence generation. In this study, one wave cycle, $\phi = 0^\circ$ to 360°, was divided into sequential eight phases as shown in Fig.10, in which trough and crest stages correspond to Phase-3 and Phase-7, respectively.

Fig.11 shows the distribution of the phase-averaged turbulence generation term $< -uv\partial U / \partial y >$, which appears in turbulent kinetic energy (TKE) equation. $< >$ indicates the phase-average operation. One recognizes negative values in the crest (Phase-3) and the trough (Phase-7). In contrast, in the falling stage of free-surface elevation (Phase-4) and the rising stage (Phase-8), positive values appear significantly. This tendency is more remarkable closer to the free-surface. Consequently, the present results revealed that turbulence is generated more significantly in the rising and falling stages, and it was also suggested that the instantaneous velocity field and coherent structure depend strongly on the phases of wave motion. These notable findings that the turbulent kinetic energy is generated in the transition between the crest and trough the consistent with the time-series of vorticity and delta distributions as shown in Figs.8 and 9.

3.7 *Decomposition of instantaneous velocity components*

Hussain & Reynolds (1970) have developed a "phase averaging technique" to decompose the instantaneous velocity component into mean, turbulence and wave motions. There exist several useful methods to decompose the instantaneous velocity components into the wave and background turbulence. Recently, the wavelet analysis is often used to compare time-series of

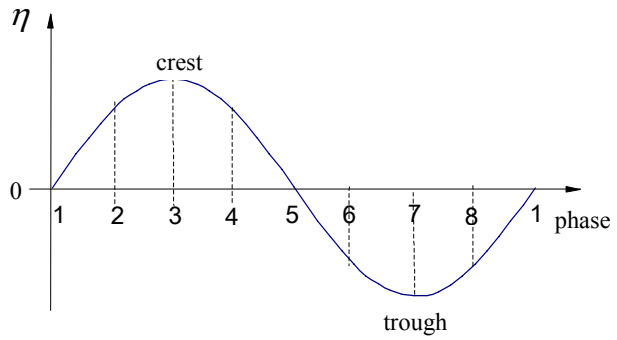

Figure 10. Phase definition using free-surface elevation

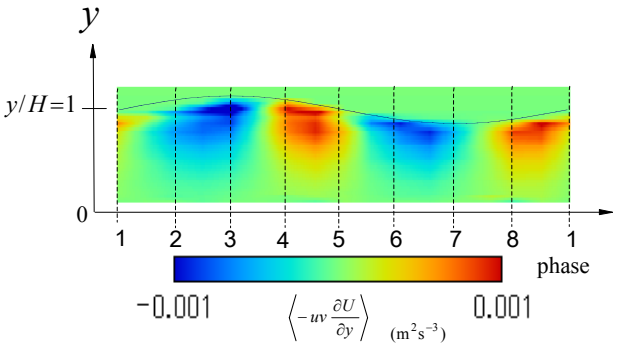

Figure 11. Phase variation of generation term of turbulent kinetic energy

measured data in different frequency bands. This enables us to conduct frequency analysis without lack of information of time variation, which is not possible with standard spectral analysis. Furthermore, wavelet analysis does not require any assumptions that other decomposition methods should consider. For example, LFT needs the condition that correlation between wave motion and turbulence should be zero. Therefore, in this study, we have used discrete wavelet analysis which yields several time-series data in lower frequency bands than the sampling rate. Applying the present technique to our measured data with sampling frequency of 50Hz, we get time-variations of velocity components in following frequency bands, i.e., 25~50Hz, 12.5~25Hz, 6.25~12.5Hz, 3.125~6.25Hz… Peak frequency of the present waves was about $f_p = 2.5$Hz. So, we defined wave motion as low frequency motion which is smaller than 3.125Hz.

Instantaneous velocity $\tilde{u}$ can be decomposed into time-averaged velocity U, velocity associated with wave motion u_w, and turbulence u_t in the following form.

$$\tilde{u} = U + u_w + u_t \quad (\because u \equiv u_w + u_t) \tag{8}$$

The Reynolds stress was also decomposed into three components as presented in Eq. (9).

$$-\overline{uv} = -\overline{u_w v_w} - \overline{u_t v_t} - \overline{u_w v_t} - \overline{u_t v_w} \tag{9}$$

Therefore, the energy loss $E = \overline{uv}\partial U/\partial y$ in the energy transport equation can be written as shown in Eq. (10).

$$E = (\overline{u_w v_w} + \overline{u_t v_t} + \overline{u_w v_t} + \overline{u_t v_w}) \times \partial U/\partial y \tag{10}$$

When a negative sign is operated to the first term at the right hand side of Eq.(10), we get $-\overline{u_w v_w}\partial U/\partial y$ which is the production term in wave kinetic energy equation (see Jiang et al. 1990). The second term becomes $-\overline{u_t v_t}\partial U/\partial y$, which is the production term in turbulent kinetic energy equation.

Fig.12 shows the vertical distributions of Reynolds stress evaluated by wave components, and background turbulence components. $-\overline{u_w v_w} < 0$ and $-\overline{u_t v_t} > 0$ are observed near the free-surface.

Since $\partial U/\partial y$ is positive in the free-surface region, the wave fluctuations supply kinetic energy to turbulence via mean flow. It is found that the contribution of interaction stress ($-\overline{u_t v_w} - \overline{u_w v_t}$) to the energy transfer is smaller than that of wave stress, and thus both of the wave stress $-\overline{u_w v_w}$ and turbulence stress $-\overline{u_t v_t}$ dominant energy transfer to the turbulence significantly.

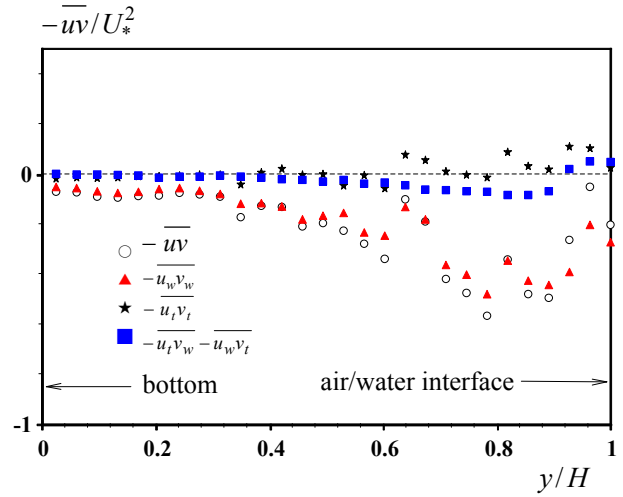

Fig.12 Vertical distributions of Reynolds stress evaluated by wave components and background turbulence components

4 CONCLUSIONS

In this study, an innovative PIV system for simultaneous measurements of velocity components and free-surface distribution was developed to examine the relation between the wave flow and turbulence near the air/water interface. The main findings obtained in this study are as follows:

1) Time variations of velocity components and free-surface elevation were evaluated simultaneously, and it was found that the streamwise velocity has the same phase as free-surface fluctuations, and in contrast, there exists a phase difference between the vertical velocity and free-surface fluctuations.

2) It was found from the present PIV that the coherent vortices appear near the air/water interface. The delta method could detect the vortex structure even in such a complex flow field. It seems that these vortices are generated associated with the reattachment of wind

flow on the wave trough as pointed out by previous studies.

3) Time variations of vorticity and delta distributions enable us to consider the transport property the coherent vortices. In particular, it was suggested that large vorticity zone exists near the crest of water waves. Furthermore, coherent vortices detected by the delta method appear in the transitional zone between the trough and crest.

4) By decomposing the instantaneous data using wavelet analysis, it was found that there exist significant energy transfers among the mean flow, turbulence and wave motion. Of particular significance is that turbulence generation is more significant at the trough than at the crest.

REFERENCES

Cheung, T.K. and Street, R.L. 1988. The turbulent layer in the water at an air-water interface. J. Fluid Mech. 194, 133-151.

Chong, M. S. and Perry, A. E. 1990. A general classification of three-dimensional flow fields, Phys. Fluids A 2(5), 765-777.

Hussain, A.K.M.F. and Reynolds, W.C. 1970. The mechanism of an organized wave in turbulent shear flow. J. Fluid Mech. 41, part2, 241-258.

Jiang, J.Y., Street, R.L. and Klots, S.P. 1990. A study on wave-turbulence interaction by use of a nonlinear water wave decomposition technique. J. Geophysical Res. 95, 16037-16054.

Komori, S., Nagaosa, R. and Murakami, Y. 1993. Turbulence structure and mass transfer across a sheared air-water interface in wind-driven turbulence. J. of Fluid Mech. 249, 161-183.

Miyamoto, H. and Kanda, T. 2002. Simultaneous image measurements of velocity field and water-surface wave in open-channel flows, Proc. Hydraulic measurement & experimental methods conference. on CD-ROM.

Oh, S.H., Mizutani, N. and Suh, K. D. 2008. Laboratory observation of coherent structures beneath microscale and large scale breaking waves under wind action, Experimental Thermal and Fluid Science 32, 1232-1247.

Okuda, K. 1982. Internal flow structure of short wind waves part1. J. Oceanogr.38, 28-42.

Rashidi, M. and Banerjee, S. 1990. The effect of boundary conditions and shear rate on streak formation and breakdown in turbulent channel flows, Phys. Fluids. A3(10), 1827-1838.

Sanjou, M., Nezu, I. and Akiya, Y. 2009. Turbulent energy transport and convection properties of flows in closed channels caused by wind-induced water waves. Proc. 33rd IAHR Congress, Vancouver. 6pages on CD-ROM.

Toba, Y. and Kawamura, H. 1996, Wind-wave coupled downward-bursting boundary layer (DBBL) beneath the sea surface, J. of Oceanogr. 52, 409-419.